Acta Oceanol. Sin., 2021, Vol. 40, No. 12, P. 125–134
https://doi.org/10.1007/s13131-021-1868-1
http://www.aosocean.com
E-mail: ocean2@hyxb.org.cn

Numerical investigation of ocean waves generated by three typhoons in offshore China

Qing Shi[1], Jun Tang[1]*, Yongming Shen[1, 2, 3, 4], Yuxiang Ma[1]

[1] State Key Laboratory of Coastal and Offshore Engineering, Dalian University of Technology, Dalian 116024, China

[2] Key Laboratory for City Cluster Environmental Safety and Green Development of the Ministry of Education, Institute of Environmental and Ecological Engineering, Guangdong University of Technology, Guangzhou 510006, China

[3] Southern Marine Science and Engineering Guangdong Laboratory (Guangzhou), Guangzhou 511458, China

[4] Guangdong Provincial Key Laboratory of Water Quality Improvement and Ecological Restoration for Watersheds, Guangzhou 510006, China

Received 17 May 2021; accepted 10 June 2021

© Chinese Society for Oceanography and Springer-Verlag GmbH Germany, part of Springer Nature 2021

Abstract

The influences of the three types of reanalysis wind fields on the simulation of three typhoon waves occurred in 2015 in offshore China were numerically investigated. The typhoon wave model was based on the simulating waves nearshore model (SWAN), in which the wind fields for driving waves were derived from the European Centre for Medium-Range Weather Forecasts (ECMWF) Re-Analysis-Interim (ERA-interim), the National Centers for Environmental Prediction climate forecast system version 2 (CFSv2) and cross-calibrated multi-platform (CCMP) datasets. Firstly, the typhoon waves generated during the occurrence of typhoons Chan-hom (1509), Linfa (1510) and Nangka (1511) in 2015 were simulated by using the wave model driven by ERA-interim, CFSv2 and CCMP datasets. The numerical results were validated using buoy data and satellite observation data, and the simulation results under the three types of wind fields were in good agreement with the observed data. The numerical results showed that the CCMP wind data was the best in simulating waves overall, and the wind speeds pertaining to ERA-Interim and CCMP were notably smaller than those observed near the typhoon centre. To correct the accuracy of the wind fields, the Holland theoretical wind model was used to revise and optimize the wind speed pertaining to the CCMP near the typhoon centre. The results indicated that the CCMP wind-driven SWAN model could appropriately simulate the typhoon waves generated by three typhoons in offshore China, and the use of the CCMP/Holland blended wind field could effectively improve the accuracy of typhoon wave simulations.

Key words: SWAN, blended wind fields, typhoon waves, three typhoons, Chan-hom, Linfa, Nangka

Citation: Shi Qing, Tang Jun, Shen Yongming, Ma Yuxiang. 2021. Numerical investigation of ocean waves generated by three typhoons in offshore China. Acta Oceanologica Sinica, 40(12): 125–134, doi: 10.1007/s13131-021-1868-1

1 Introduction

Typhoon waves are most damaging ocean disasters and always cause considerable damage to coastal engineering, ship navigation and marine engineering applications. Study on the influences of wind fields on evolution of the typhoon wave are important for accurate modelling typhoon waves and providing supports for ocean and coastal disaster prevention and mitigation.

Several studies on numerical simulations of typhoon waves by using different wind data have been conducted (Zhang et al., 2011; Liang et al., 2016, 2019; Zhou et al., 2016; Shao et al., 2018; Wang et al., 2018; Mo et al., 2019). Zhang et al. (2011) simulated the wave process in the Bohai Sea by using the simulating waves nearshore model (SWAN), in which the wind data from the cross-calibrated multi-platform (CCMP) was used as the driving wind field. Liang et al. (2016) investigated the wave climate of the Bohai Sea, Yellow Sea, and East China Sea for the period from 1990 to 2011 by using the SWAN wave model, and the wind parameters were obtained from the weather research and forecasting (WRF) model. Wang et al. (2018) investigated the extreme wave climate variability in the South China Sea (SCS) by using the WAVEWATCH III, and the wind data was using the objective reanalysis wind dataset from the WRF model. Li et al. (2018) utilized ERA-interim reanalysis wind data from the European Centre for Medium-Range Weather Forecasts (ECMWF) to simulate the waves and surges over the northwest Pacific region for a 35-year period. Liang et al. (2019) studied the characteristics of global waves simulated by using SWAN model driven by the ERA-Interim wind database from 1979 to 2017. Zhou et al. (2016) simulated typhoon waves by using the WAVEWATCH III model driven by the National Centers for Environmental Prediction (NCEP) Final Analysis (FNL) wind field during the occurrence of typhoons Chan-hom (1509), Linfa (1510) and Nangka (1511) in 2015. To improve the accuracy of typhoon waves, the combined

Foundation item: The Key Special Project for Introduced Talents Team of Southern Marine Science and Engineering Guangdong Laboratory (Guangzhou) under contract No. GML2019ZD0403; the Program for Guangdong Introducing Innovative and Enterpreneurial Teams under contract No. 2019ZT08L213; the Guangdong Provincial Key Laboratory Project under contract No. 2019B121203011.

*Corresponding author, E-mail: jtang@dlut.edu.cn

wind fields based on reanalysis wind data and theoretical wind model, such as Holland wind model (Holland, 1980), have also been used for driving wave models. Shao et al. (2018) simulated 29 tropical cyclones (TCs) in the South China Sea (SCS) and East China Sea (ECS) by using the SWAN wave model driven by ERA-Interim wind data, Holland theoretical model and blended model wind data, and the results showed that the blended wind model demonstrated better performance than that of both the ERA-interim and the Holland model. Compared to the progress of numerical simulations of typhoon waves caused by a single typhoon, the simulations of typhoon waves in a unique weather background involving multiple typhoons have still not been well investigated. The evolution of the typhoon waves generated by multiple typhoons are more complex and difficult to predict than those generated by a single typhoon, and it is crucial to study the influences of wind fields on typhoon waves caused by multiple simultaneous typhoons.

The present study intended to perform a numerical study of the typhoon waves in offshore China under the influence of three typhoons where the wind fields for driving waves were derived respectively from the ERA-interim, climate forecast systerm version 2 (CFSv2) and CCMP datasets. The remaining paper is organized as follows. Section 2 presents the principle of the wave model, modelling data and model setup used in the study. Section 3 presents the validation results pertaining to the occurrence of three typhoons in offshore China in 2015 against altimetry and buoy data. In addition, the investigation concerning the improvement of the wind field, and the comparison of the accuracy of the wave field simulation before and after wind field correction is discussed. The conclusions are presented in Section 4.

2 Numerical model and setup

2.1 *Wave model and wind data*

SWAN and WAVEWATCH III are the efficient third-generation wave models for modelling waves driven by winds in which wave generation, refraction and dissipation due to whitecapping and breaking etc. are considered. WAVEWATCH III model is usually applied for modelling ocean waves, and SWAN model considering more nearshore physical processes is more suitable for modelling offshore waves. In the study, SWAN model is applied for modelling typhoon waves in China offshore zones. The equation for the SWAN wave model is based on the spectral action balance equation and can be expressed in Cartesian coordinates as (Booij et al., 1996)

$$\frac{\partial N}{\partial t}+\frac{\partial C_x N}{\partial x}+\frac{\partial C_y N}{\partial y}+\frac{\partial C_\sigma N}{\partial \sigma}+\frac{\partial C_\theta N}{\partial \theta}=\frac{S_{\mathrm{tot}}}{\sigma}, \tag{1}$$

$$N(\sigma,\theta)=\frac{E(\sigma,\theta)}{\sigma}, \tag{2}$$

where $N(\sigma,\theta)$ is the action density, $E(\sigma,\theta)$ is the energy density, σ represents the frequency, θ is the wave direction, C_x and C_y are the propagation velocities of the wave energy in spatial space, and C_σ and C_θ are the propagation velocities in the spectral space caused respectively by the change in current and water depth. These parameters can be expressed as the following:

$$\begin{pmatrix} C_x \\ C_y \end{pmatrix}=\begin{pmatrix} \frac{1}{2}\left(1+\frac{2|\vec{k}|h}{\sinh\left(2|\vec{k}|h\right)}\right)\frac{\sigma\vec{k}}{|\vec{k}|^2}\cdot\vec{i}+\vec{U}\cdot\vec{i} \\ \frac{1}{2}\left(1+\frac{2|\vec{k}|h}{\sinh\left(2|\vec{k}|h\right)}\right)\frac{\sigma\vec{k}}{|\vec{k}|^2}\cdot\vec{j}+\vec{U}\cdot\vec{j} \end{pmatrix}, \tag{3}$$

$$C_\sigma=\frac{\partial\sigma}{\partial h}\left(\frac{\partial h}{\partial t}+\vec{U}\cdot\nabla_{\vec{x}}h\right)-C_{\mathrm{g}}\vec{k}\cdot\frac{\partial\vec{U}}{\partial s}, \tag{4}$$

$$C_\theta=-\frac{1}{|\vec{k}|}\left(\frac{\partial\sigma}{\partial h}\frac{\partial h}{\partial m}+\vec{k}\cdot\frac{\partial\vec{U}}{\partial m}\right), \tag{5}$$

$$\nabla_{\vec{x}}=\left(\frac{\partial}{\partial x},\frac{\partial}{\partial y}\right), \tag{6}$$

where $\vec{C_{\mathrm{g}}}$ is the wave group velocity, $\vec{U}$ is the current velocity, $\vec{k}$ is the unit vector, h is the water depth, s is the space coordinate along the θ direction, and m is the space coordinate perpendicular to θ.

S_{tot} is the source term that represents all physical processes which generate, including the wind energy input, white capping, depth-induced wave breaking, non-linear wave-wave interaction, bottom friction dissipation. The source term can be expressed as

$$S_{\mathrm{tot}}=S_{\mathrm{in}}+S_{\mathrm{ds,w}}+S_{\mathrm{ds,b}}+S_{\mathrm{ds,br}}+S_{\mathrm{nl4}}+S_{\mathrm{nl3}}, \tag{7}$$

where S_{in} represents the wind energy input (Phillips, 1957; Miles, 1957), $S_{\mathrm{ds,w}}$ represents whitecapping, $S_{\mathrm{ds,b}}$ is the bottom friction dissipation term, $S_{\mathrm{ds,br}}$ represents depth-induced wave breaking, S_{nl4} represents the quadruplet wave-wave interactions, and S_{nl3} represents the triad wave interaction. The present study focused mainly on typhoon waves, and the wind energy input are the main source term. The wind energy input item S_{in} can be expressed as

$$S_{\mathrm{in}}(\sigma,\theta)=A+BE(\sigma,\theta), \tag{8}$$

where A represents linear growth and B represents exponential growth. The expression for the term A was obtained from Cavaleri and Rizzoli (1981):

$$A=\frac{1.5\times10^{-3}}{2\pi g^2}[U_*\cdot\max(0,\cos(\theta-\theta_{\mathrm{w}}))]^4H, \tag{9}$$

$$H=\exp\left[-\left(\frac{\sigma}{\sigma^*_{\mathrm{PM}}}\right)^{-4}\right], \tag{10}$$

$$\sigma^*_{\mathrm{PM}}=\frac{0.13g}{28U_*}2\pi, \tag{11}$$

where U_* is the frictional velocity, θ_{w} is the wind direction, H is the filter used to avoid exponential growth of low-frequency waves, and σ^*_{PM} (Pierson and Moskowitz, 1964) is the peak frequency of the fully developed sea state. The expression of B was obtained from Komen et al. (1984):

$$B = \max\left[0, 0.25\frac{\rho_a}{\rho_w}\left(28\frac{U_*}{c_{ph}}\cos(\theta-\theta_w)-1\right)\right]\sigma, \quad (12)$$

where c_{ph} is the phase speed; and ρ_a and ρ_w denote the densities of air and water, respectively. The white-capping item $S_{ds,w}$ can be defined by (Hasselmann, 1974):

$$S_{ds,w} = -\Gamma\bar{\sigma}\frac{k}{\bar{k}}E(\sigma,\theta), \quad (13)$$

where Γ is the coefficient related to wave steepness. The bottom friction dissipation term $S_{ds,b}$ is defined by:

$$S_{ds,\,b} = -c_b\frac{\sigma^2}{g^2\sinh kd}E(\sigma,\theta), \quad (14)$$

where $c_b = 0.038\ m^2/s^3$ is the bottom friction coefficient. The depth-induced wave breaking term $S_{ds,\,br}$ can be defined by (Battjes and Janssen, 1978):

$$S_{ds,\,br} = \frac{D_{tot}}{E_{tot}}E(\sigma,\theta), \quad (15)$$

where $D_{tot} = -\frac{1}{4}\alpha_{BJ}Q_b\left(\frac{\bar{\sigma}}{2\pi}\right)H_{max}$, and Q_b is defined as $\frac{1-Q_b}{\ln Q_b} = -8\frac{E_{tot}}{H_{max}^2}$.

The expressions for quadruplet wave-wave interaction term S_{nl4} and the triad wave interaction term S_{nl3} can be found in the references Hasselmann et al. (1985) and Eldberky and Battjes (1995).

In the SWAN model, an accurate wind field is the basis for simulating of the wind driven waves. Nowadays, a variety of reanalysis wind fields have been widely used, such as ERA-interim, CFSv2 and CCMP dataset (Stopa and Cheung, 2014; Wang et al., 2016; Pan et al., 2016). ERA-interim utilizes the 4-Dimensional Variational Data assimilation scheme in wind reanalysis, and this system contains a coupled wave-atmosphere component, and the wave model assimilates the altimeter observations (Stopa, 2018). The CFSv2 was executed in 2011, and it has demonstrated improvement in the product, especially in the tropical regions, with an increased resolution of 22 km (T574) (Saha et al., 2014). CFSv2 uses the 3-Dimensional Variational Data assimilation with assimilations being updated every 6 h (Stopa, 2018). The CCMP dataset (Atlas et al., 2011) is provided by the Physical Oceanographic Data Distribution Archives Center of National Aeronautics and Space Administration (NASA), and it uses the reanalysis and operational data of ECMWF as the background field. Studies have shown that CCMP has a considerably higher accuracy than wind field data measured by other single satellite platforms (Atlas et al., 2008).

2.2 *Modelling area and model setup*

ETOPO1 global topographic and bathymetric data (Amante and Eakins, 2009) with a resolution of 1′ can satisfy the requirements of global sea wave simulations. The modelling area is 0°–40°N, 105°–145°E, which covers in offshore China area. The tracks of the three typhoons Chan-hom (1509), Linfa (1510) and Nangka (1511) occurred in 2015 are shown in Fig. 1. A total of four buoys were placed in the Yellow Sea, East China Sea and South China Sea, and the bathymetry and buoy positions in the calculation area are shown in Fig. 2. The buoy data is referenced from Zhou et al. (2016).

In the simulation, the range of wave direction was 0°–360°, which was divided into 36 grids. The range of frequency was 0.04–1.00 Hz. The resolution of the computing grid in space was 0.1°, and the self-nesting mode of SWAN based on the regular structured model was used to verify the buoy data (no nesting is required when verifying satellite data) as the buoys are close to the coast. The accuracy of the nested computing grid in space was 0.02°. The wind input, non-linear interaction, bottom friction dissipation, depth-induced wave breaking and wave diffraction were taken into account. First, the SWAN model was driven via ERA-Interim, CFSv2 and CCMP wind fields. The period of calculation was from 00:00 on July 1, 2015 to 18:00 on July 18 (UTC).

3 Simulation of typhoon waves during three typhoons

The Pearson correlation coefficient, mean deviation (Bias) and root mean square error (RMSE) were used for data deviation analysis. The parameters of the evaluation used for verification included the significant wave height obtained from buoy observation and the significant wave height and wind speed obtained from Jason-2 observation. Here, X_{SL} represents the calculated results and X_{MEA} denotes the buoy altimetry or satellite data. The relevant expressions are as follows:

$$\text{Bias} = \frac{1}{n}\sum_{1}^{n}(X_{SL} - X_{MEA}), \quad (16)$$

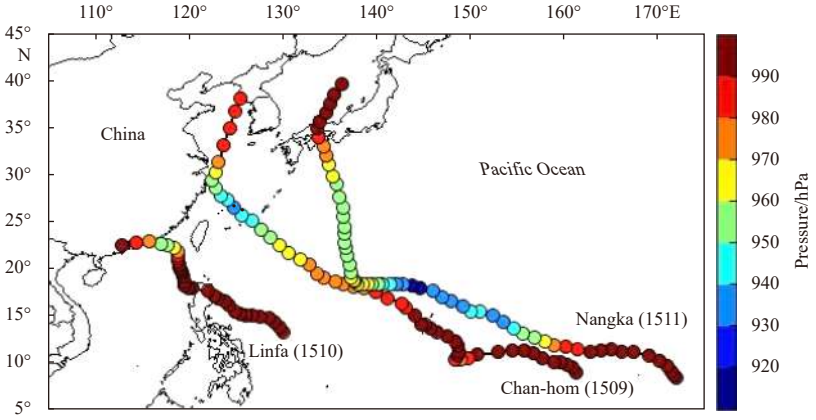

Fig. 1. Tracks of the three typhoons in 2015.

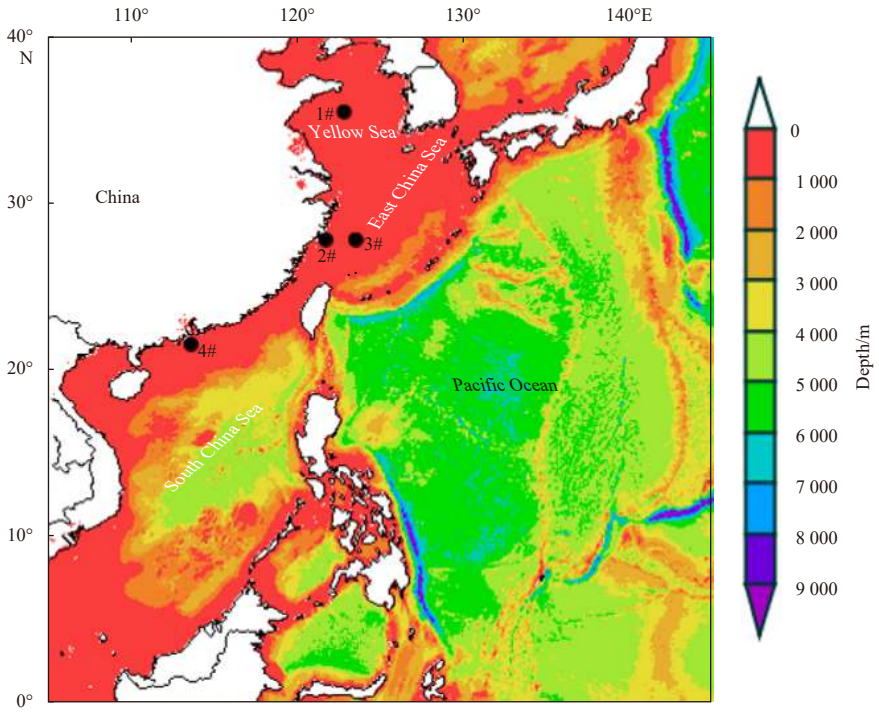

Fig. 2. Bathymetry and positions of the buoys.

$$\mathrm{RMSE} = \sqrt{\frac{1}{n}\sum_{1}^{n}(X_{\mathrm{SL}} - X_{\mathrm{MEA}})^2}. \tag{17}$$

The simulated wave height at different buoys during the three typhoons were compared with the observed data, and the results are shown in Fig. 3 and Table 1. It can be seen that the correlation coefficients of the simulation results of two buoys driven by the three wind fields in the East China Sea are as much as 0.966, and the correlation coefficient of Buoy 1# in the Yellow Sea is also larger than 0.8. This means that the typhoon waves during the three typhoons driven by the ERA-Interim, CFSv2 and CCMP wind fields, could be simulated well overall. The calculated wave height at Buoy 4# at the South China Sea is close to that observed, but the correlation coefficient is relatively low compared with those at other buoys. This may be due to that Buoy 4# is very close to the shallow coast and the water depth around it is relatively shallow, and errors always get larger when getting closer to the coast. These lead to the correlation coefficient of the Buoy 4# in the South China Sea being lower than the correlation coefficients for buoys in the Yellow Sea and East China Sea. Generally, for a small wave height, the simulated wave heights driven by CCMP wind field are closer to the measured values, and the simulated wave heights driven by ERA-Interim and CFSv2 wind fields are smaller. For a large wave height, the simulated wave heights driven by CFSv2 wind field demonstrates the best performance, while the simulated wave heights driven by CCMP ERA-Interim and CCMP wind fields are smaller. According to the interaction between wind and waves, large winds usually generate large waves. It can be inferred that the wind speeds near the typhoon centre in the study area, pertaining to the ERA-Interim and CCMP wind fields, are smaller than the actual values. The CCMP wind field is more reasonable when the wind speed is low.

In combination with the analysis presented in Table 1, the absolute values of the Bias and RMSE of Buoy 2# are determined to be less than 0.2 m, which represents the best performance. The Bias and RMSE of Buoy 4# are small. Buoy 3# presents remarkably satisfactory trends, with the maximum absolute values of Bias and RMSE being 0.796 m and 1.038 m, owing to the large wave height. The overall simulation results for Buoy 1# can be considered moderate, as determined by the characteristics of the original wind field.

To further verify the model, the altimetry and sea surface wind speed obtained from Jason-2 as it passed through the simulated sea during the occurrence of typhoon waves were adopted. The data accuracy is high owing to the high orbit accuracy of GDR (geographical data record) and the waveform being recorrected. The satellite trajectory points were divided into three categories: those pertaining to the Yellow Sea (31°–39°N, 119°–127°E), the East China Sea (23°–31.18°N, 117.18°–131°E) and the South China Sea (4°–23°N, 105°–119°E). The detailed verification results are shown in Fig. 4.

The significant wave height products observed by Jason-2 include those pertaining to the Ku-band and C-band. In the product specification of OSTM/Jason-2 in 2011, Ku-band observations are better than C-band. Therefore, the study used Ku band data with a data accuracy of 0.001 m (Wang et al., 2016). The comparison results of Jason-2 presented in Table 2 show that the correlation coefficients of the simulated wave height and wind speed between the satellite observations are relatively big under the three wind fields. The correlation coefficients of the wave height and wind speed reach up to 0.969 and 0.971. Even at the South China Sea, the correlation coefficients are larger than 0.7. Overall, the trend of the wave height is similar to that of the wind speed, and this is also consistent with that obtained by Zhou et al. (2016). The results show that the RMSEs of the wave height in the Yellow Sea and South China Sea are smaller than 1 m. The maximum wave height in the East China Sea is as much as 12 m, and the RMSE of the wave height is larger. This is mainly attribute to the deviation of simulated wind speed in the East

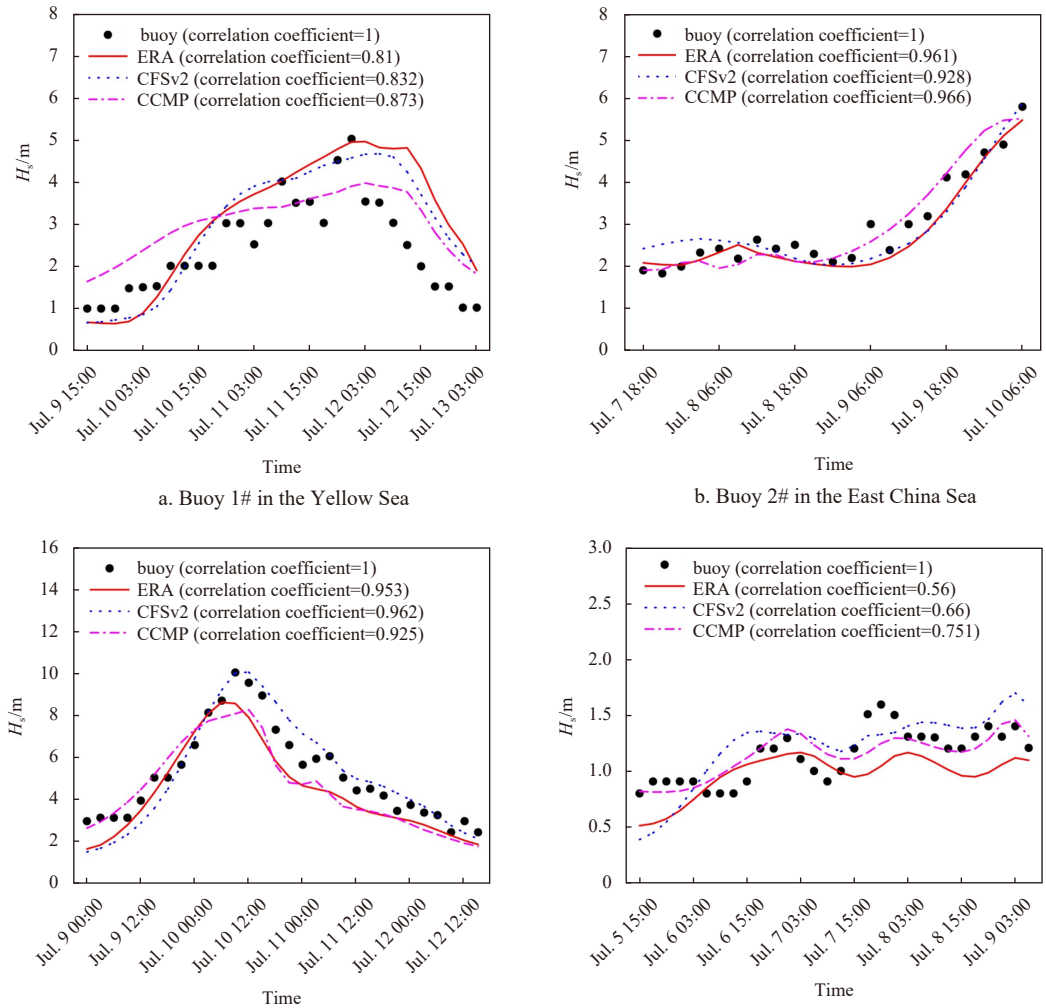

Fig. 3. Verification of wave height of the four buoys.

Table 1. Deviation of wave height between simulated data and buoys

Buoy	Deviation of wave height			
	Parameter	ERA-Interim	CFSv2	CCMP
1#	CC	0.810	0.832	0.873
	Bias/m	0.703	0.558	0.592
	RMSE/m	1.121	0.965	0.840
2#	CC	0.810	0.832	0.873
	Bias/m	–0.196	–0.034	0.041
	RMSE/m	0.129	0.170	0.116
3#	CC	0.953	0.962	0.925
	Bias/m	–0.796	0.035	–0.623
	RMSE/m	1.037	0.788	1.038
	CC	0.560	0.660	0.751
4#	Bias/m	–0.165	0.085	0.008
	RMSE/m	0.261	0.261	0.154

China Sea. Moreover, the track of typhoon Chan-hom (1509) is close to the coast in the East China Sea and the waves are deeply influenced by the complicated coastal topography and shorelines, and the measurement errors of satellite data are also bigger than those in the open ocean zones, which may also cause the relative large simulation deviation in the East China Sea. However, the trend of the wave heights in the East China Sea fit quite well with the observed results and those obtained by Zhou et al. (2016). The wind field comparison results indicate that the CCMP wind field fits the satellite observation better, followed by the fitting of the CFSv2 wind field. The CFSv2 wind field data is slightly larger, and the CCMP wind field and CFSv2 wind field are closer to the satellite data than the ERA-Interim wind field is.

To study the typhoon waves corresponding to three typhoons

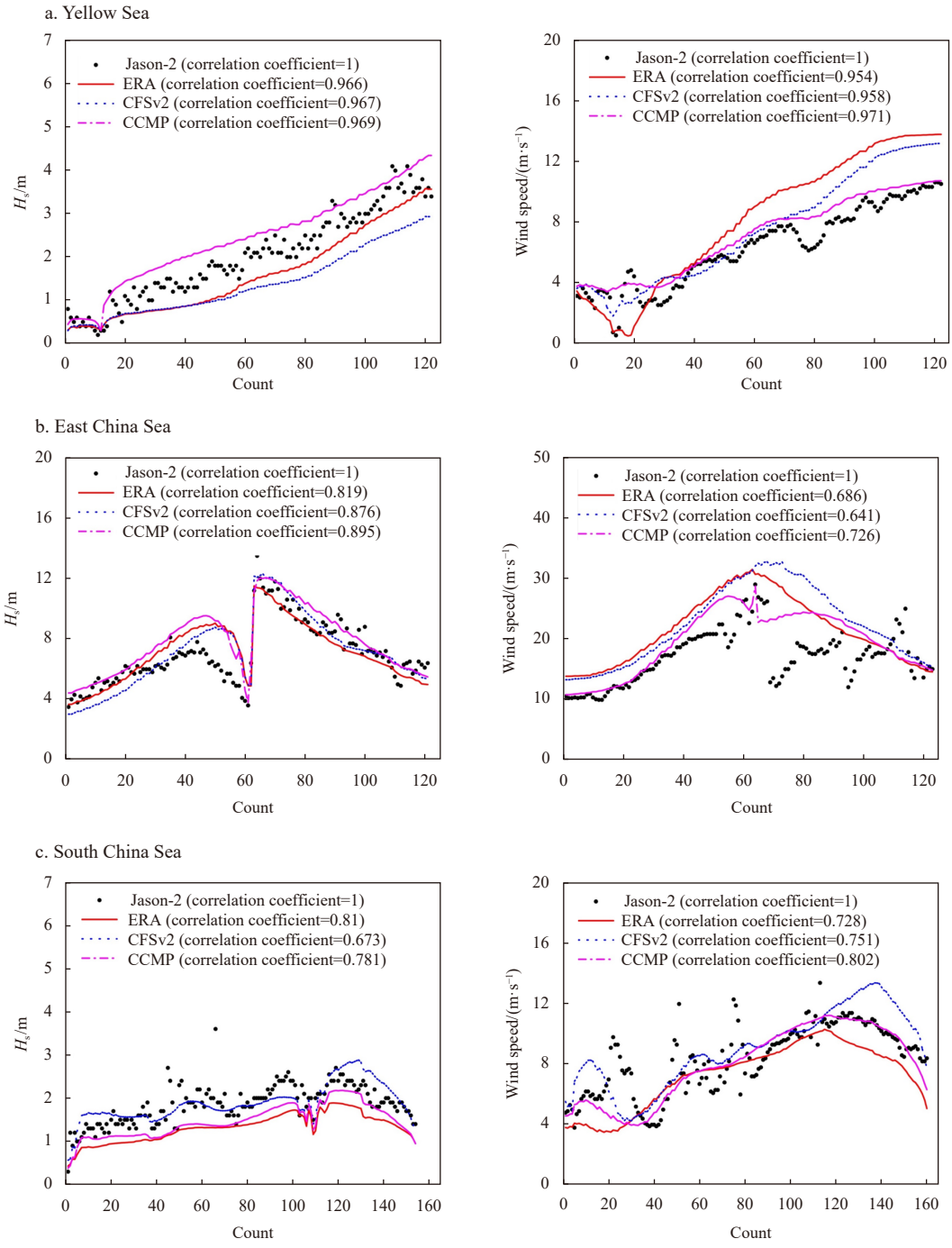

Fig. 4. Validation of wave height and wind speed of satellite in the Yellow Sea (a; 31°–39°N, 119°–127°E), the East China Sea (b; 23°–31.18°N, 117.18°–131°E) and the South China Sea (c; 4°–23°N, 105°–119°E).

accurately, it is necessary to verify the accuracy of the description of the typhoon centres. The maximum average wind speed near the centre of the three typhoons (the maximum average wind speed pertaining to the three wind fields at the corresponding time) and the best track values (http:www.tcdata.typhoon.org.cn) (2014) were compared, and the results are shown in Fig. 5.

It can be seen from Fig. 5 that the values of the maximum wind speed pertaining to the CFSv2 wind field, for which the correlation coefficients are larger than 0.85, is the most close to the best track values, whereas the wind speeds pertaining to the ERA-Interim and CCMP wind fields are notably smaller in comparison.

To accurately simulate the waves during three typhoons, the CCMP wind field, which demonstrated the best performance in terms of the wave height and wind speed in the simulation of typhoon waves in three typhoons that occurred in 2015, was selected as the background wind field, and it was blended with the Holland theoretical wind model (1980) to overcome the shortcomings of CCMP, these shortcomings include the wind speed near the typhoon centre being small and the deviation of the typhoon centre. The Holland model (Holland, 1980) is a theoretical wind field model based on the exponential distribution of the

Table 2. Deviation of wave heigh and wind speed between simulated data and Jason-2

Area	Parameter	Deviation of wave height			Deviation of wind speed		
		ERA-Interim	CFSv2	CCMP	ERA-Interim	CFSv2	CCMP
Yellow Sea	CC	0.966	0.967	0.969	0.954	0.958	0.971
	Bias/m	–0.415	–0.483	0.423	1.872	1.236	0.773
	RMSE/m	0.491	0.714	0.495	2.700	1.800	0.995
East China Sea	CC	0.819	0.876	0.895	0.686	0.641	0.726
	Bias/m	0.148	0.010	0.838	4.400	5.400	2.400
	RMSE/m	1.232	1.176	1.281	6.000	7.100	4.400
South China Sea	CC	0.810	0.673	0.781	0.728	0.751	0.802
	Bias/m	–0.420	0.005	–0.413	–0.536	0.040	–0.389
	RMSE/m	0.618	0.337	0.509	0.597	0.355	0.479

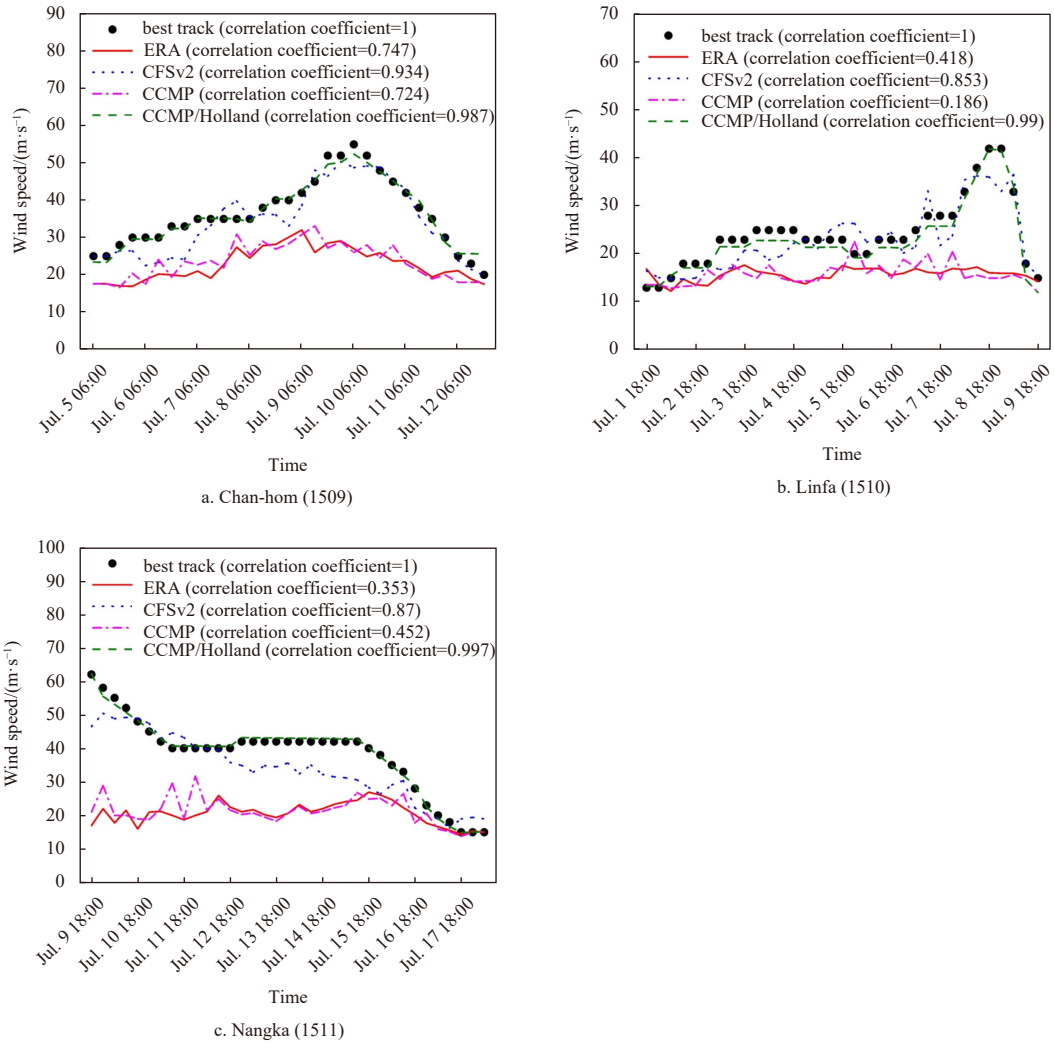

Fig. 5. Maximum wind speed near the centre of typhoon of Chan-hom (1509), Linfa (1510), Nangka (1511).

atmospheric pressure field defined by Schloemer (1954) and a peak parameter B, and it can be expressed as follows:

$$P = P_c + (P_n - P_c)\exp\left(-\frac{R_{max}^B}{r^B}\right), \tag{18}$$

$$U_g = \sqrt{\frac{B}{\rho_a}\left(\frac{R_{max}}{r}\right)^B (P_n - P_c)\exp\left[-\left(\frac{R_{max}}{r}\right)^B\right] + \left(\frac{rf^2}{2}\right)} - \frac{rf}{2}, \tag{19}$$

$$R_{max} = 28.52\tanh\left[0.087\,3(\varphi - 28)\right] + 12.22\exp\left(\frac{P_c - P_n}{33.86}\right) + 0.2V_f + 37.2, \tag{20}$$

$$B = 1.5 + \frac{980 - P_c}{120}, \tag{21}$$

where U_g represents the gradient wind speed at radius r, f is the Coriolis force parameter, P_n is the atmospheric pressure around the typhoon, P_c is the atmospheric pressure at the typhoon

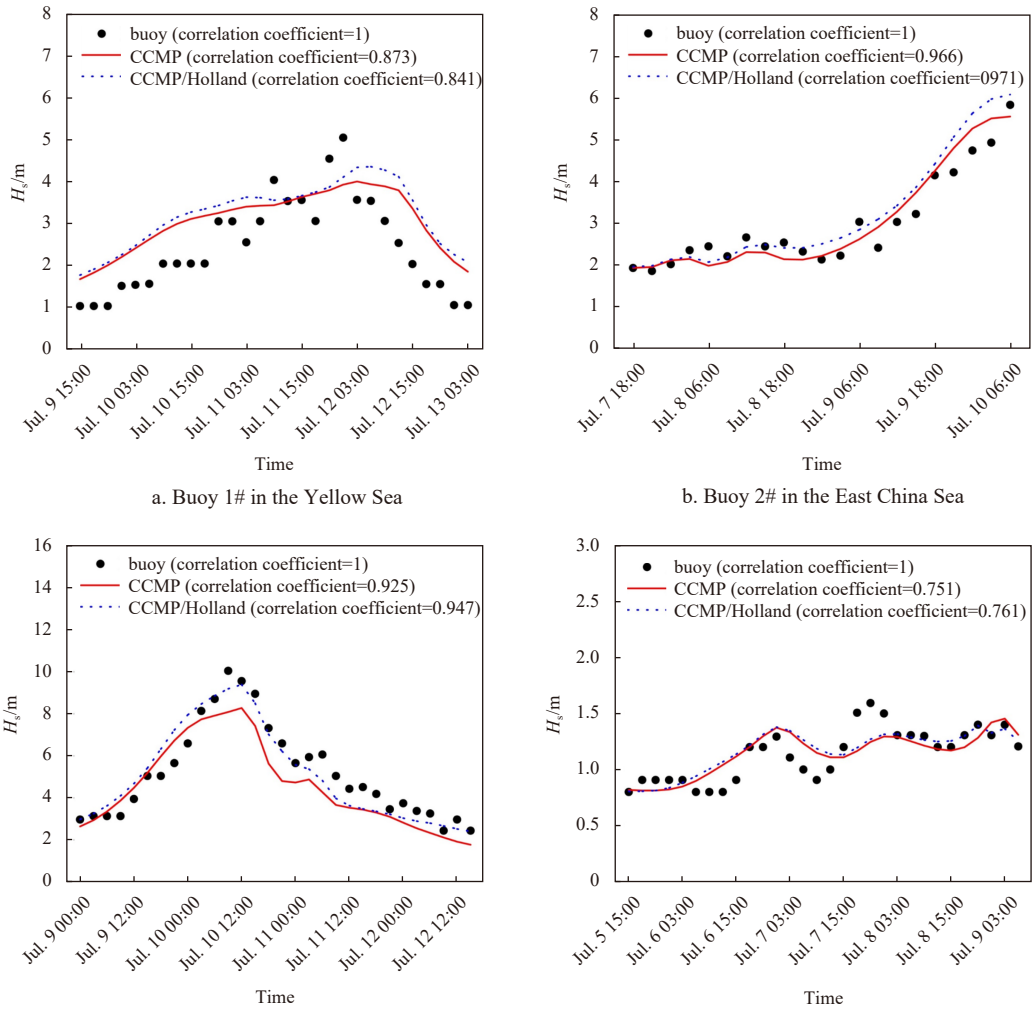

Fig. 6. Simulated wave height of the four buoys before and after correction of wind.

centre, $R_{\max}$ is the maximum wind speed radius and B is the parameter defined by Hubbert et al. (1991).

The combined scheme can be defined with reference to Wang et al. (2017). First, according to the position of the typhoon centre, the radius of the circle that pertains to the most similar wind speed of the theoretical wind field and that of the CCMP wind field was determined as the reference superposition radius R. R_1 and R_2 denote the characteristic superposition radius. R_1 is determined from the inward L_1 distance and R_2 is determined from the outward L_2 distance based on R. To ensure smooth integration of the theoretical wind field and CCMP reanalysis of the wind field, L_1 and L_2 are generally defined to be between $0.05R$ and $0.15R$. The superposition formula can be defined as follows:

$$\begin{cases} V_x = V_{Hx}, \\ V_y = V_{Hy}, \end{cases} \quad r < R_1, \tag{22}$$

$$\begin{cases} V_x = \alpha V_{\mathrm{CCMP}x} + (1-\alpha)\, V_{Hx}, \\ V_y = \alpha V_{\mathrm{CCMP}y} + (1-\alpha)\, V_{Hy}, \end{cases} \quad R_1 \leqslant r < R_2, \tag{23}$$

$$\begin{cases} V_x = V_{\mathrm{CCMP}x}, \\ V_y = V_{\mathrm{CCMP}y}, \end{cases} \quad r \geqslant R_2, \tag{24}$$

$$\alpha = \frac{r - R + L_1}{L_1 + L_2}, \tag{25}$$

where V_x and V_y represent the components of the superimposed wind speed in the x and y directions, respectively. V_{Hx} and V_{Hy} represent the components of Holland wind speed in the x and y directions, respectively; and $V_{\mathrm{CCMP}x}$ and $V_{\mathrm{CCMP}y}$ represent the components of the CCMP wind speed in the x and y directions, respectively.

To adjust the wind speed to the standard 10-m elevation above the sea surface, multiplication by a correction factor K should be performed. In the present study, the K values for Chanhom, Linfa and Nangka were determined to be 0.82, 0.78 and 0.78, respectively. The superimposed radius R was 2.3 times the maximum typhoon radius. Next, a blended wind field was used to drive the SWAN model, and the comparison between the simulated wave heights driven by the blended wind field and those driven by the CCMP is shown in Fig. 6.

From Fig. 6, it can be seen that the simulated wave height driven by the blended wind field is mostly consistent with the buoy data, and the simulated maximum wave height due to the blended wind field is more consistent with the buoy data. It can be concluded that the blended wind field overcomes a limitation of the CCMP which the wind speed near the centre of typhoon is

too small, and the simulated wave driven by the blended wind is more accurate.

In conclusion, the above mentioned verification results obtained using observation data from buoys and satellites indicate that the present model is suitable for modelling waves caused by three typhoons in offshore China. It is found that the simulated wave height driven by the CCMP wind field is closer to buoy data overall, and the RMSE is smaller in this case. When the wave height is small, the simulated wave heights driven by the CCMP wind field are close to the measured data, and the simulated wave heights driven by both ERA-Interim and CFSv2 are smaller than the measured data; when the wave height is large, the simulated wave heights driven by the CFSv2 wind field agree best with the measured data, and those driven by the ERA-Interim and CCMP wind fields are smaller than the measured data. It can be concluded that the wind speed of the CCMP wind field far from the centre of typhoon is more reasonable; in addition, this observation is consistent with the results from Kuang et al. (2015). It is further noted that the maximum wind speed near the typhoon centre of the ERA-Interim and CCMP wind fields is significantly smaller than the corresponding best track value. For the wind speed near the centre of the typhoon, the blended wind field constructed by using the CCMP-superimposed Holland model is more reasonable. The simulated maximum wave height driven by the blended wind field is more reasonable.

4 Conclusions

The influences of the three types of wind fields on typhoon wave simulations were numerically investigated. The typhoon waves driven by the ERA-Interim, CFSv2 and CCMP reanalysis wind fields were simulated via SWAN considering three typhoons that occurred in offshore China in 2015. Next, the maximum wind speeds near the typhoon centres during three typhoons that occurred in 2015 were evaluated by comparing the values with the best track data. Furthermore, the simulated wave heights driven by the CCMP and CCMP/Holland blended wind fields during three typhoons that occurred in 2015 were analysed. The following conclusions could be obtained.

(1) The typhoon waves in offshore China during the three typhoons, driven by the ERA-Interim, CFSv2 and CCMP wind fields, could be simulated well overall. The simulated wave heights driven by the CCMP wind field were more accurate for small waves. The simulated wave heights driven by the CFSv2 wind fields were more accurate for large waves, and the simulated wave heights driven by the ERA-Interim and CCMP wind field were relatively smaller than the measured data. The maximum wind speeds near the typhoon centre of the three typhoons that occurred in 2015 were compared with the best track data, and it was found that the wind speeds of the ERA-Interim, CFSv2 and CCMP wind fields were relatively smaller than the corresponding best track values.

(2) Moreover, the CCMP/Holland blended wind field was noted to be superior to the CCMP wind field for the simulation of extremely large wave heights. Furthermore, the wind speed pertaining to the CCMP wind field near the centre of the typhoon was relatively small, and the position and moving track of the typhoon eye were deviated. The CCMP/Holland blended wind field could overcome these shortcomings and effectively improve the simulation accuracy of the wave field, especially for extreme waves.

References

Amante C, Eakins B W. 2009. ETOPO1 1 arc-minute global relief model: procedures, data sources and analysis. Boulder: NOAA, doi: 10.7289/V5C8276M

Atlas R, Ardizzone J, Hoffman R N. 2008. Application of satellite surface wind data to ocean wind analysis. In: Proceedings Volume 7087, Remote Sensing System Engineering. San Diego: International Society for Optical Engineering, 70870B

Atlas R, Hoffman R N, Ardizzone J, et al. 2011. A cross-calibrated, multiplatform ocean surface wind velocity product for meteorological and oceanographic applications. Bulletin of the American Meteorological Society, 92(2): 157–174, doi: 10.1175/2010BAMS2946.1

Battjes J A, Janssen J P F M. 1978. Energy loss and set-up due to breaking of random waves. In: 16th International Conference on Coastal Engineering. Hamburg: American Society of Ciril Engineers, 569–587

Booij N, Holthuijsen L H, Ris R C. 1996. The "SWAN" wave model for shallow water. In: 25th International Conference on Coastal Engineering. Orlando: American Society of Ciril Engineers, 668–676

Cavaleri L, Rizzoli P M. 1981. Wind wave prediction in shallow water: theory and applications. Journal of Geophysical Research: Oceans, 86(C11): 10961–10973, doi: 10.1029/JC086iC11p10961

Eldberky Y, Battjes J A. 1995. Parameterization of triad interactions in wave energy models. In: Proceeding Coastal Dynamics Conference '95. Gdańsk: ASCE, 140–148

Hasselmann K. 1974. On the spectral dissipation of ocean waves due to white capping. Boundary-Layer Meteorology, 6(1): 107–127

Hasselmann S, Hasselmann K, Allender J H, et al. 1985. Computations and parameterizations of the nonlinear energy transfer in a gravity-wave specturm: Part Ⅱ. Parameterizations of the nonlinear energy transfer for application in wave models. Journal of Physical Oceanography, 15(11): 1378–1391, doi: 10.1175/1520-0485(1985)015<1378:CAPOTN>2.0.CO;2

Holland G J. 1980. An analytic model of the wind and pressure profiles in hurricanes. Monthly Weather Review, 108(8): 1212–1218, doi: 10.1175/1520-0493(1980)108<1212:AAMOTW>2.0.CO;2

Hubbert G D, Holland G J, Leslie L M, et al. 1991. A real-time system for forecasting tropical cyclone storm surges. Weather and Forecasting, 6(1): 86–97, doi: 10.1175/1520-0434(1991)006<0086:ARTSFF>2.0.CO;2

Komen G J, Hasselmann S, Hasselmann K. 1984. On the existence of a fully developed wind-sea spectrum. Journal of Physical Oceanography, 14(8): 1271–1285, doi: 10.1175/1520-0485(1984)014<1271:OTEOAF>2.0.CO;2

Kuang Fangfang, Zhang Youquan, Zhang Junpeng, et al. 2015. Comparison and evaluation of three sea surface wind products in Taiwan Strait. Haiyang Xuebao (in Chinese), 37(5): 44–53

Li Jiangxia, Pan Shunqi, Chen Yongping, et al. 2018. Numerical estimation of extreme waves and surges over the northwest Pacific Ocean. Ocean Engineering, 153: 225–241, doi: 10.1016/j.oceaneng.2018.01.076

Liang Bingchen, Gao Huijun, Shao Zhuxiao. 2019. Characteristics of global waves based on the third-generation wave model SWAN. Marine Structures, 64: 35–53, doi: 10.1016/j.marstruc.2018.10.011

Liang Bingchen, Liu Xin, Li Huajun, et al. 2016. Wave climate hindcasts for the Bohai Sea, Yellow Sea, and East China Sea. Journal of Coastal Research, 32(1): 172–180

Miles J W. 1957. On the generation of surface waves by shear flows. Journal of Fluid Mechanics, 3(2): 185–204, doi: 10.1017/S0022112057000567

Mo Dongxue, Liu Yahao, Hou Yijun, et al. 2019. Bimodality and growth of the spectra of typhoon-generated waves in northern South China Sea. Acta Oceanologica Sinica, 38(11): 70–80, doi: 10.1007/s13131-019-1500-9

Pan Yi, Chen Yongping, Li Jiangxia, et al. 2016. Improvement of wind field hindcasts for tropical cyclones. Water Science and Engineering, 9(1): 58–66, doi: 10.1016/j.wse.2016.02.002

Phillips O M. 1957. On the generation of waves by turbulent wind. Journal of Fluid Mechanics, 2(5): 417–445, doi: 10.1017/S0022

112057000233

Pierson Jr W J, Moskowitz L. 1964. A proposed spectral form for fully developed wind seas based on the similarity theory of S. A. Kitaigorodskii. Journal of Geophysical Research, 69(24): 5181–5190, doi: 10.1029/JZ069i024p05181

Saha S, Moorthi S, Wu Xingren, et al. 2014. The NCEP climate forecast system version 2. Journal of Climate, 27(6): 2185–2208, doi: 10.1175/JCLI-D-12-00823.1

Schloemer R W. 1954. Analysis and Synthesis of Hurricane Wind Patterns Over Lake Okeechobee, Florida. Washington: Weather Bureau, Department of Commerce and US Army Corps of Engineers

Shao Zhuxiao, Liang Bingchen, Li Huajun, et al. 2018. Blended wind fields for wave modeling of tropical cyclones in the South China Sea and East China Sea. Applied Ocean Research, 71: 20–33, doi: 10.1016/j.apor.2017.11.012

Stopa J E. 2018. Wind forcing calibration and wave hindcast comparison using multiple reanalysis and merged satellite wind datasets. Ocean Modelling, 127: 55–69, doi: 10.1016/j.ocemod.2018.04.008

Stopa J E, Cheung K F. 2014. Intercomparison of wind and wave data from the ECMWF reanalysis interim and the NCEP climate forecast system reanalysis. Ocean Modelling, 75: 65–83, doi: 10.1016/j.ocemod.2013.12.006

Wang Qisong, Deng Jiaquan, Liu Cheng, et al. 2017. Application of superimposed wind fields to the hindcast modelling of typhoon-induced waves in the South China Sea. Haiyang Xuebao (in Chinese), 39(7): 70–79

Wang Juanjuan, Gao Zhiyi, Wang Jiuke, et al. 2016. Validation on Jason-2 significant wave height product for China seas. Oceanologia et Limnologia Sinica (in Chinese), 47(3): 509–517

Wang Zhifeng, Li Shuiqing, Dong Sheng, et al. 2018. Extreme wave climate variability in South China Sea. International Journal of Applied Earth Observation and Geoinformation, 73: 586–594, doi: 10.1016/j.jag.2018.04.009

Zhang Peng, Chen Xiaoling, Lu Jianzhong, et al. 2011. Research on wave simulation of Bohai Sea based on the CCMP remotely sensed sea winds. Marine Science Bulletin (in Chinese), 30(3): 266–271

Zhou Yuanyuan, Zhou Lin, Guan Hao. 2016. Numerical simulation of typhoon waves in the Northwest Pacific Ocean. Marine Forecast (in Chinese), 33(5): 23–30